SPE-171788-MS

Wettability Alteration by Asphaltene Deposition: A Field Example

Takaaki Uetani, INPEX Corporation

This paper was prepared for presentation at the Abu Dhabi International Petroleum Exhibition and Conference held in Abu Dhabi, UAE, 10–13 November 2014.

Abstract

Description: Identifying and understanding wettability alteration caused by asphaltene deposition, and its implications for field development optimization is growing in interest. In this paper, we present a field case study on the cause of an unexpected decline in reservoir productivity and simultaneous rapid increase in water production. We concluded that the decline in productivity and water cut increase were caused by asphaltene precipitation in the formation with a subsequent increase in the water relative permeability. This was caused by alteration of rock wettability from water-wet to oil-wet by asphaltene deposition.

Applications: This work's findings can improve understanding of reservoir performance and help optimize reservoir management strategies for oil reservoirs with potential asphaltene precipitation problems.

Results and Conclusions: All possible parameters in the reservoir simulation model was thoroughly examined and discussed. Switching the relative permeability type from water-wet toward oil-wet at the asphaltene onset pressure (AOP) yielded an excellent history match with the observed rapid water production increase. The reservoir had been depleted following primary production; the laboratory PVT data indicated that the AOP was a little below the initial reservoir pressure and hence asphaltene precipitation had been predicted.

Technical Contributions: This work contributes to (1) providing a field case bridging asphaltene deposition and wettability alteration, (2) understanding phenomena such as rapid increase in water production associated with asphaltene deposition, and (3) optimizing reservoir management and field development for oil reservoirs with potential asphaltene precipitation problems.

Introduction

Twice in its production history, a well (Well B) in the central region of a Japanese oil field 'M' (**Fig. 1**) exhibited an unexpected decline in productivity and simultaneous rapid increase in water cut (**Fig. 2**). The first case was observed from 2008 to 2010. Productivity dropped immediately after a matrix acidizing job in March 2008, when the skin factor increased from 7 to 40. Rapid water cut increase was also observed, rising from 2-3% to 10-15%. The productivity recovered significantly in January 2011 when xylene was injected into the formation. The improved productivity following the xylene treatment was accompanied by a decrease in the water cut back to 2-3%. We concluded that asphaltene sludging as a result of the

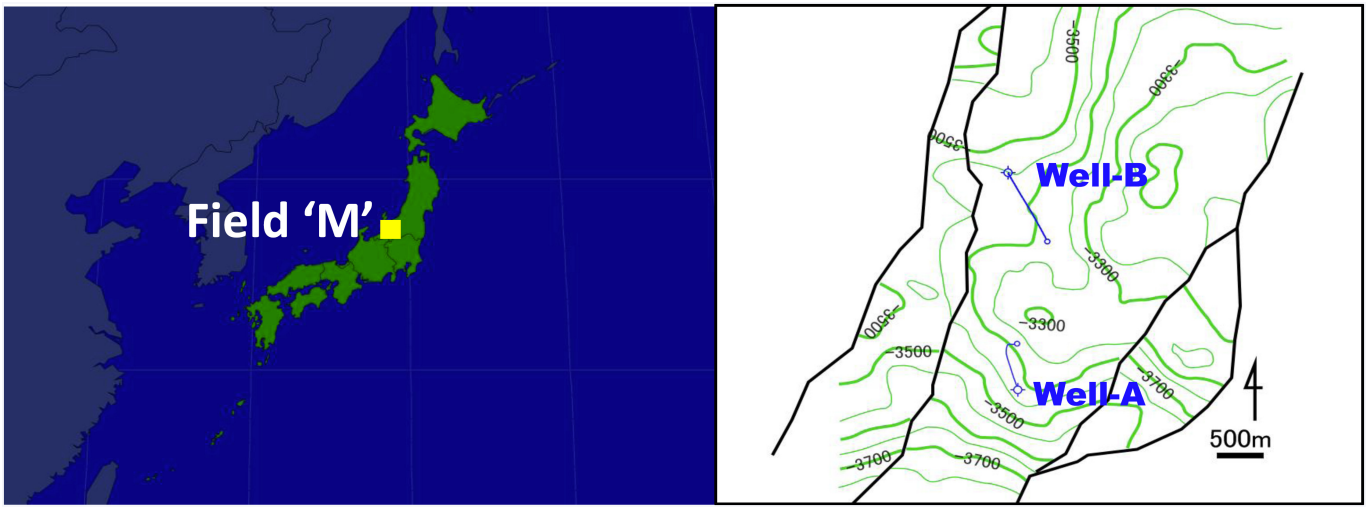

Figure 1—Location of Field 'M' in the central region of Japan (left). Structural features of the reservoir (right). Green lines represent structural contours (subsea depths in meters). Bold black lines represent faults. Wells are shown in blue. There is no pressure communication between Wells A and B.

unsuccessful acid treatment was the cause of the formation damage. While the cause of the rapid increase in water cut was unclear, we suspected a correlation between asphaltene precipitation and increase in water cut.

The second reduction in productivity was observed in early 2013 and is ongoing as of April 2014. After the xylene treatment in January 2011, Well B entered a pseudo-steady state with a constant oil production rate from 2011 to 2012, and associated water cut of approximately 3%. The pseudo-steady state ended unexpectedly when the flowing bottomhole pressure was approximately 4,700 psia; productivity declined and water cut rapidly increased even though the oil production rate was fixed. A reservoir material balance study indicated negligible aquifer influx, as shown in **Fig. 3**, indicating the reservoir was the source of the water.

The main objective of this study was to find the causes of the productivity decline and rapid water cut increase in Well B observed since early 2013. Several potential causes were investigated including the precipitation of asphaltene, increase in water relative permeability due to wettability alteration by asphaltene deposition, weak aquifer influx, inorganic scale precipitation, and water influx from behind the casing. This paper presents pressure transient analysis, laboratory work and numerical simulation studies.

Field Investigation

Increasing skin was observed in the two pressure buildup surveys conducted in September 2013 and February 2014. The log-log diagnostic plot (**Fig. 4**) shows that the skin factor increased from 3.0 to 4.5, while the reservoir flow capacity (*kh*) remained constant. This suggests that the cause of the decline in the productivity may be linked to formation damage around the wellbore. Flowing bottomhole pressures immediately before the well shut-ins were 3,421 psia in September 2013 and 3,218 psia in February 2014.

Experimental Investigation

Asphaltene Precipitation

Asphaltenes, which are known to cause problems in oil fields (Leontartis and Mansoori 1987; Mansoori 1988; Kokal 1995) are widely found in Well B from bottomhole to surface and serious asphaltene problems have been reported in Field 'M' (Uetani, et al. 2013). **Fig. 5** shows asphaltenes deposits on the production logging tool that was run in Well B.

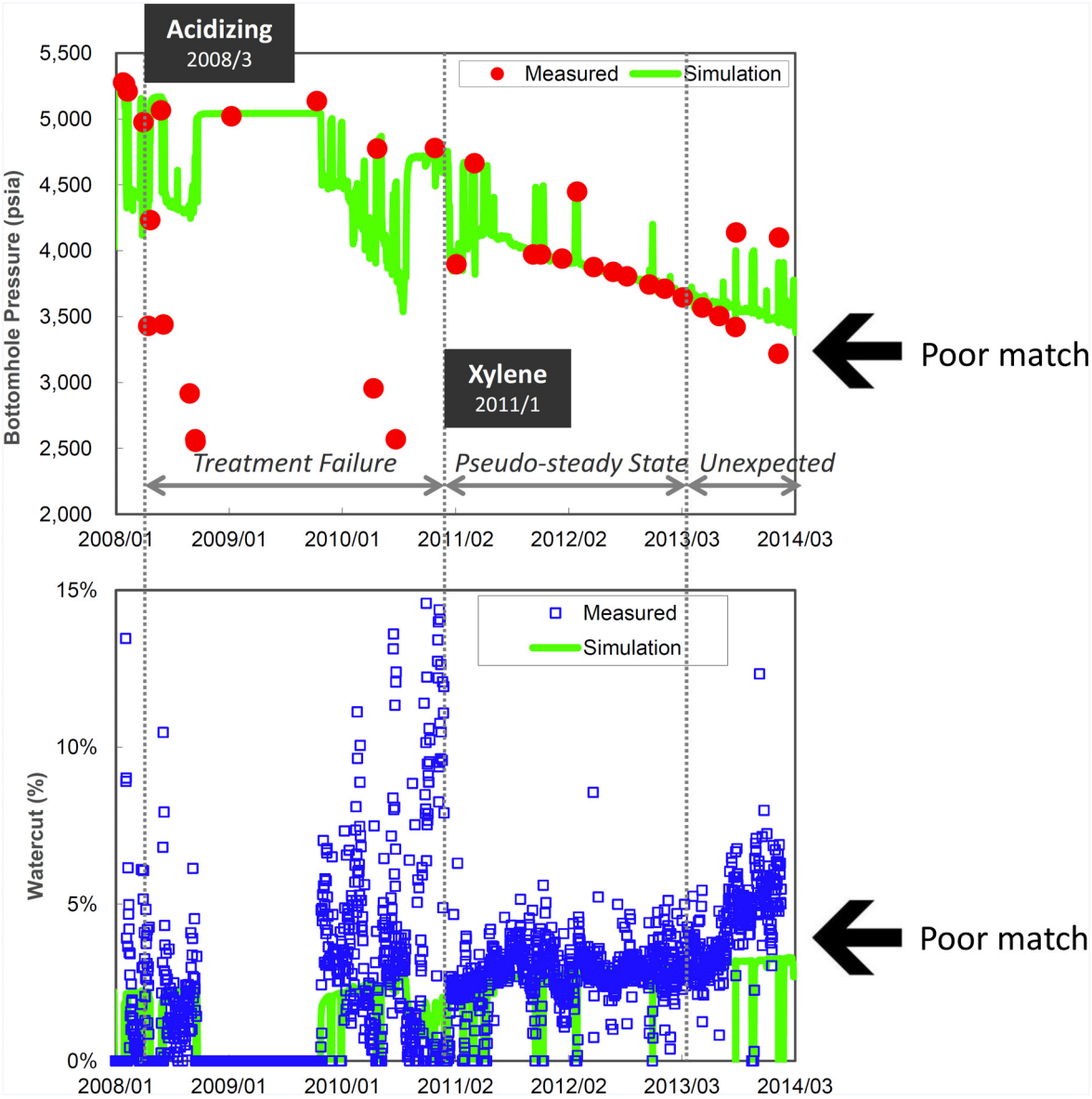

Figure 2—Bottomhole pressure (top) and water cut (bottom) for Well B. Red dots represent measured pressure. Blue dots represent daily measured water cut. Green lines represent pressure or water cut results calculated by the reservoir simulation, which does not include the effect of asphaltene. The matches are poor from 2008 to 2010 due to the acid treatment failure in March 2008. A good match is achieved from 2011 to 2012 after a xylene treatment in January 2011. There is a clear discrepancy between the observed data and the simulation is from early 2013 onward.

Laboratory measurements using a near infrared (NIR) light-scattering technique (Jamaluddin et al. 2002) indicated the asphaltene onset pressure (AOP) of the single-phase bottomhole sample from Well B was 3,410 psia, at the reservoir temperature of 150°C (**Fig. 6**). The bubble point pressure was observed at 1,720 psia, which was consistent with our previous PVT laboratory test.

Below the AOP, the size of the precipitated asphaltene exceeded 20 μm below the AOP, which is larger than the maximum pore throat radius. Precipitated asphaltene particles were visualized using high pressure microscopy (HPM), and the images were analyzed. The laboratory equipment and the measurement principle are detailed elsewhere (Akbarzadeh et al 2007; Hammami and Ratulowski 2007). The particle size distributions and the images at different pressures are presented in **Fig. 7**. For comparison, pore size distributions of the core samples measured by mercury injection technique from Well B are illustrated in **Fig. 8**. The data suggest that asphaltene plugging can occur inside the porous media when pressure drops below the AOP.

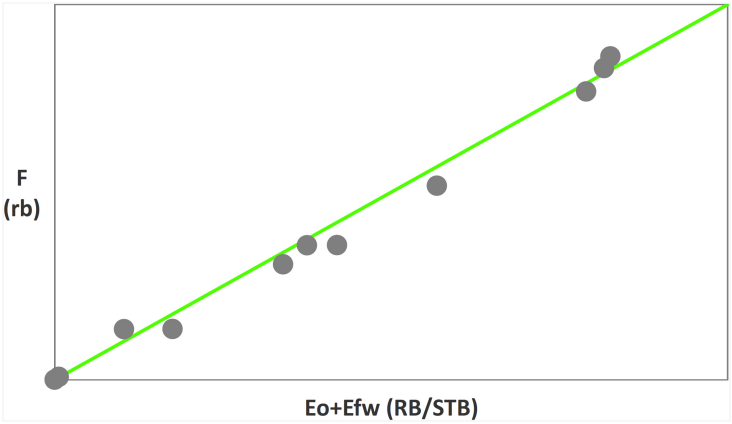

Figure 3—Havlena and Odeh material balance plot for Well B. Plotted points fall on a straight line, indicating that aquifer influx is negligible. F represents the underground withdrawal, E_o represents the expansion of oil, and E_{fw} represents the expansion of the initial water and the reduction in the pore volume.

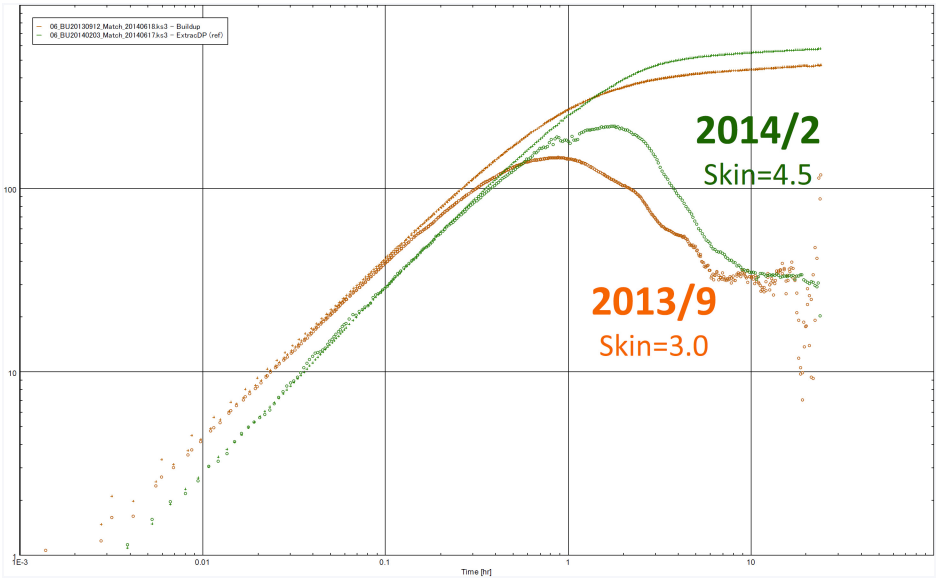

Figure 4—Time-lapse pressure-transient data for Well B. Increasing skin is indicated between September 2013 and February 2014, while the flow capacity (kh) remained constant.

The measured AOP (3,410 psia) was close to the flowing bottomhole pressure when the productivity decline started in early 2013 (approximately 3,700 psia). This suggests that the cause of the productivity decline is most likely linked to asphaltene precipitation.

Filtration Test

A filtration test was conducted to determine the solubility of asphaltene as a function of pressure at the reservoir temperature. The filtration test procedure is detailed in Jamaluddin et al. (2002). Data obtained from the experiment using a 0.5 μm high-pressure filter is shown in **Fig. 9**. The AOP was inferred to be 4,829 psia, which was higher than the

Figure 5—Asphaltenes found on the production logging tool after its survey in Well B in April 2011.

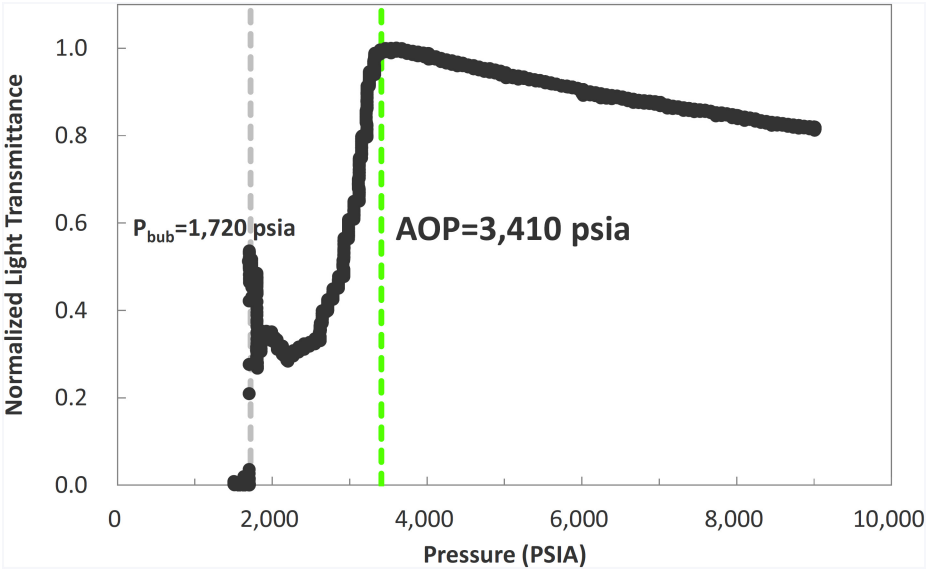

Figure 6—Near infrared light-scattering response at reservoir temperature. The results indicated that the AOP is 3,410 psia and the bubble point pressure is 1,720 psia.

result from the NIR light-scattering measurement (3,410 psia). This may be because the filtered asphaltene particles were too small to be detected by the NIR instrument. The result of the filtration test was later adjusted and used as input data for the reservoir simulation model.

Table 1—XRD Analysis

Rock Mineralogy	Weight%
Quartz	52-81%
Plagioclase	13-37%
Clays	5-13%
Potassium feldspar	0-4%
Pyrite	0-1%

Compatibility Test with Injected Acid

Well B's productivity dropped sharply after the matrix acidizing job performed in March 2008, in which a mixture of hydrochloric and hydrofluoric acids (HCl-HF) was injected into the formation. The well's productivity improved significantly when xylene was injected in 2011. HCl-HF acid can cause severe asphaltene sludging (Houchin et al. 1990) but no laboratory compatibility test was performed prior to the acid stimulation job. We conducted a laboratory test to investigate the compatibility between Well B's crude oil and the injected acid. The result showed that a large amount of asphaltene sludge was formed, as shown in **Fig. 10**. We also found that more than 90% of the sludge was soluble in xylene. Based on the compatibility test, we concluded that the cause of the sharp decline in productivity after the matrix acidizing in March 2008 was most likely asphaltene sludging, and that the well productivity recovered because these sludges were removed by the xylene treatment. Flowing bottomhole pressure before the acid injection was estimated to be approximately 4,400 psia, which is higher than the AOP of 3,410 psia. Asphaltene would not precipitate naturally at this pressure regime.

Colloidal Instability Index

Well B's asphaltene precipitation tendency was estimated to be "severe" using the colloidal instability index (CII), suggested by Yen, Yin, and Asomaning (2009). The CII is expressed as the ratio of the sum of saturates and asphaltenes to the sum of resins and aromatics (Eq. 1).

$$\mathrm{CII} = \frac{Saturates + Asphaltenes}{Resins + Aromatics} \quad (1)$$

Oils with a CII below 0.7 are considered to be stable, while those above 0.9 are highly unstable. The CII values calculated for the oil sample from Well B was 2.6, indicating that the asphaltene precipitation

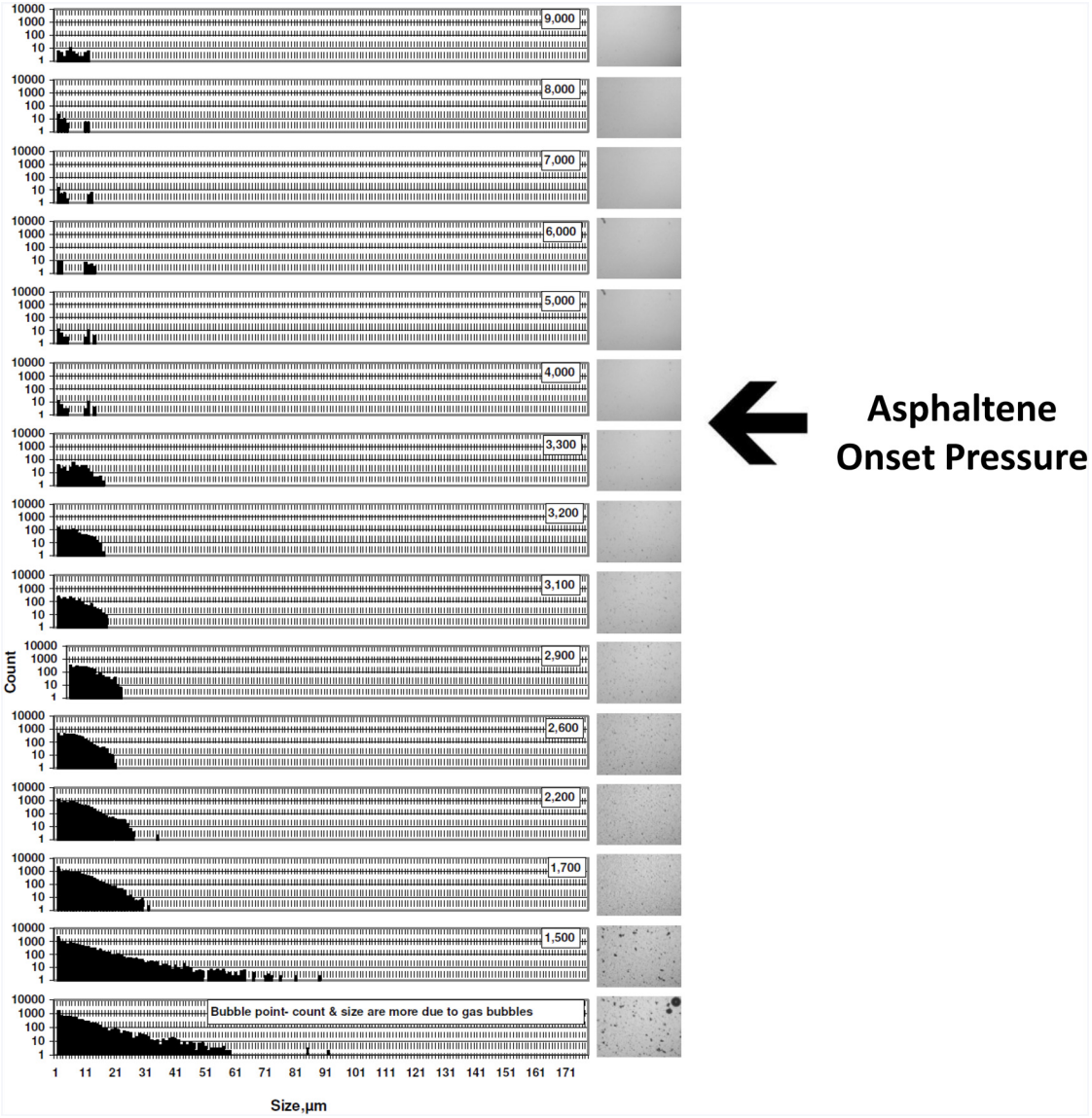

Figure 7—Particle size analysis (left) and photomicrographs (right) during discrete stepwise depressurization (from 9,000 psig to 1,400 psig) at the reservoir temperature. The AOP can be inferred to lie between 4,000 psig and 3,300 psig.

tendency of the Well B fluid is severe, even though the fraction of asphaltene is small (0.9 weight%). **Fig. 11** shows results of saturates, aromatics, resins, and asphaltenes (SARA).

Molecular Structure of Asphaltene Fractions

The average molecular structure of asphaltene fraction from the Well B oil sample was constructed based on the Brown-Ladner method (Brown and Ladner 1960). Graphical representation of the molecular structure (**Fig. 12**) shows the average asphaltene molecule has polarity due to the presence of hetero-atoms and condensed aromatic rings (Pedroza et al. 1995). Note also that it has both polar and hydrocarbon ends. We extracted the asphaltene fraction by precipitation in heptane and conducted a series of laboratory experiments including gel permeation chromatography (GPC) mean molecular weight analysis, CHNS elemental analysis, and nuclear magnetic resonance (NMR) analysis. The composition of the average asphaltene molecule is $C_{46.3}H_{43}N_1S_{0.2}O_{0.9}$, with a molecular weight of 634. Details of the experiments and data interpretation are provided in Tagami et al. (2014) and Hibi et al. (2014).

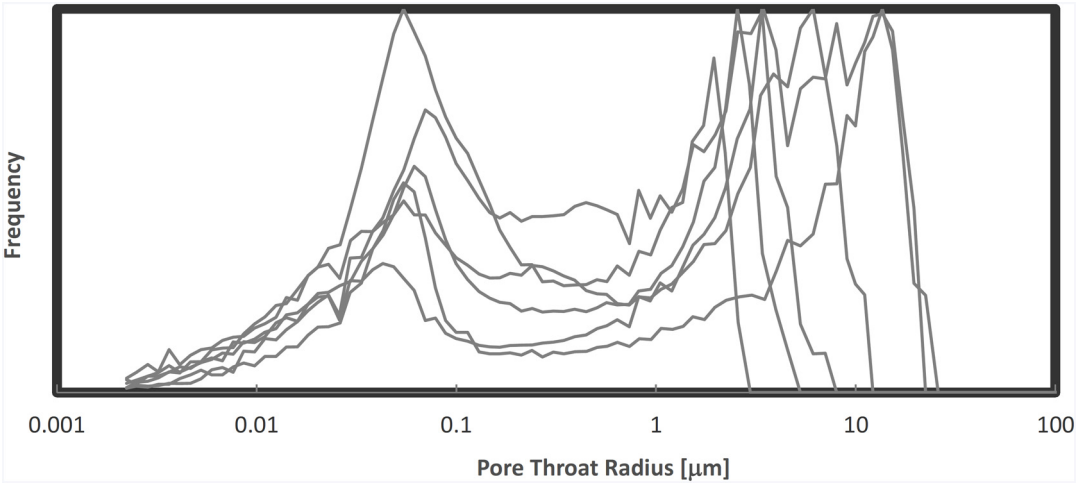

Figure 8—Pore size distributions of the six core samples from the sandstone reservoir of Well B. The bimodal distributions show both macro-pores and micro-pores.

Rock Mineralogy

Well B produces oil from the clay-rich Pliocene turbidite-sandstone. X-ray diffraction (XRD) analysis of 22 core samples showed that the most common minerals are quartz and plagioclase, followed by clays, potassium feldspar and pyrite, as summarized in **Table 1**. Clay minerals are mostly comprised of illite/smectite and iron rich chlorite.

Scanning electron microscope (SEM) images of a core sample (**Fig. 13**) show that the clay minerals occur with grain-coating and pore-filling habits. These images are consistent with the bimodal pore size distributions shown in Fig. 8. In general, rocks with large amounts of clay (and therefore high surface area) exhibit high irreducible water saturations (Morgan and Gordon, 1970).

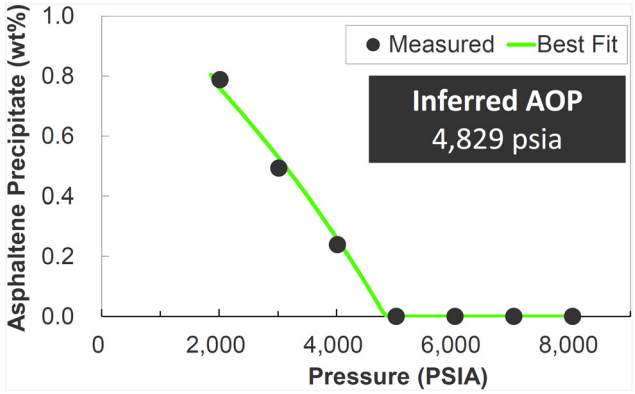

Figure 9—Filtration test conducted at reservoir temperature. The AOP was inferred to be 4,829 psia.

Original Wettability

The original wettability of the reservoir rock was inferred to be water-wet for three reasons: First, connate water saturation in the production intervals estimated from the well log interpretation are in the range 50-70%. According to Craig's rules of thumb (Craig 1993), water-wet rocks usually exhibit water saturation (S_w) greater than 20-25%, while oil-wet rocks are frequently less than 10%. Laboratory measurement of the irreducible water saturations by centrifuge and porous plate were also in the range 50-70% using 17 cleaned core samples.

Second, in water-oil relative permeability curves obtained from five restored-state core samples (**Fig. 14**), the oil and water curves cross at S_w of 50-75%. According to Craig's rules of thumb, oil and water relative permeabilities usually cross at S_w greater than 50% in water-wet rocks, while in oil-wet rocks they cross at S_w less than 50%. The five data sets also exhibited maximum oil relative permeabilities that were greater than the maximum water relative permeability, which is also an indication of water-wet rocks (Anderson 1987).

Third, the initial reservoir pressure (approximately 5,200 psia) was greater than the AOP measured by NIR light-scattering (3,410 psia). It is believed that the Well B reservoir rock was deposited in aqueous environments into which oil later migrated. Asphaltene would not precipitate because the original pressure

Figure 10—Asphaltene sludge precipitated after mixing oil from Well B with acids that were injected into the formation in March 2008.

is higher than the AOP, and the connate water would prevent the oil from touching the rock surfaces (Anderson 1986).

Water Salinity

Water production from non-perforated intervals, as a result of casing leak, was considered as a possible cause of the rapid increase in water cut. If this were true, then the salinity of the produced water should change. However, water salinity has been constant since the production startup, as illustrated in **Fig. 15**. Therefore, water from behind the casing was excluded from the investigation.

Inorganic Scaling

Inorganic scaling was considered as a possible cause of the decline in productivity. However, the potential for inorganic scaling was considered to be negligible for the following reasons: Total dissolved solids (TDS) of the produced water was only 5,737 ppm, indicating negligible scaling potential. The laboratory water analysis is summarized in **Table 2**; No scaling has been observed in Well B, either at bottomhole or at the surface; and the operator does not inject water into Well B so there is no chance of introducing an incompatible brine.

Discussion

The results from the experimental investigation suggest the productivity decline during 2008-2010 is most likely linked to asphaltene precipitation as a result of the unsuccessful acid treatment in March 2008. Productivity recovered because the asphaltene sludges were removed by xylene in January 2011. The productivity decline observed since early 2013 is probably linked to asphaltene precipitation as a result of the natural pressure depletion, in which the reservoir pressure dropped below the AOP.

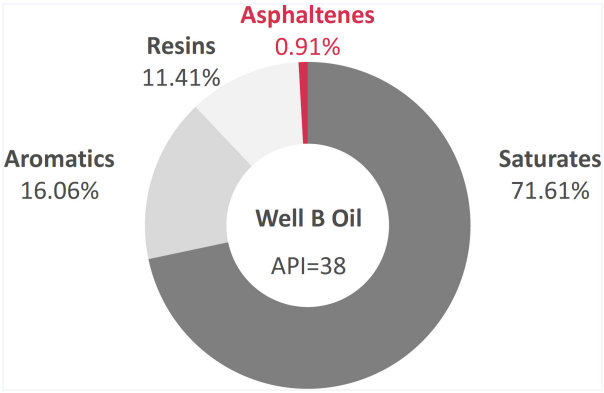

Figure 11—SARA analysis shows the content of asphaltene is low.

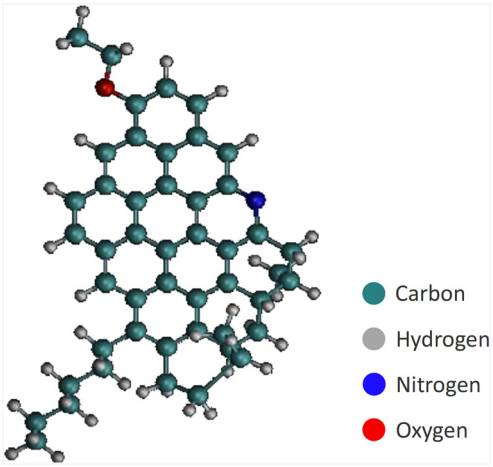

Figure 12—Average molecular structure of Well B's asphaltene fraction. The molecule has polarity due to the presence of heteroatoms and condensed aromatic rings. The sulphur fraction is negligible and so is not shown.

It is well known that asphaltene deposition on rock surfaces causes wettability alteration from water-wet to oil-wet (Anderson 1986; Kaminsky and Radke 1997; Nghiem and Kohse 2006), and consequently affects the relative permeability (Anderson 1987). The mechanism of wettability alteration by asphaltene deposition is described below, and illustrated in **Fig. 16**. Originally, the negatively charged silica surface is covered by a film of water, attached by hydrogen bonding (Pallatt and Thornley 1990).

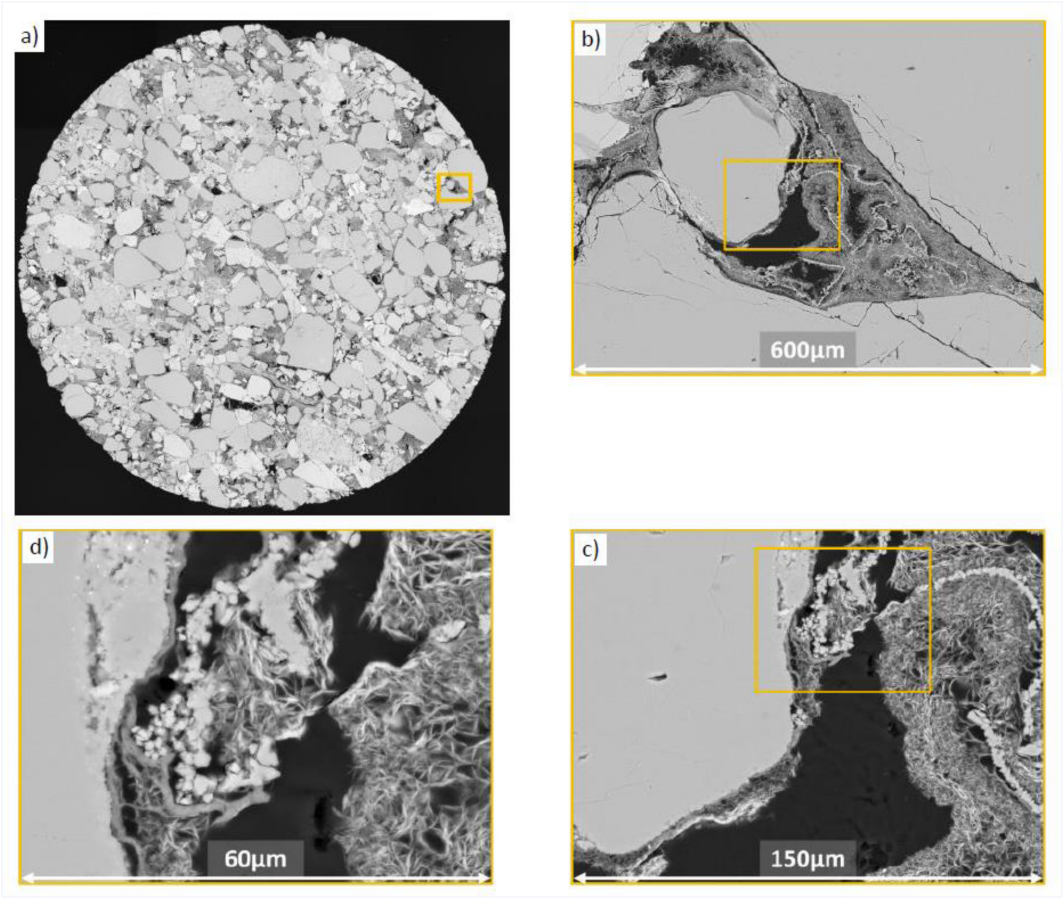

Figure 13—SEM images of a core sample from Well B at different magnifications show details of grain-coating and pore-filling clays. Permeability of the sample is 0.5 mD and porosity is 15.3%.

When the reservoir pressure is higher than the AOP, asphaltene molecules are believed to be surrounded and stabilized by resins that act as peptizing agents (Hammami and Ratulowski 2007). Once the reservoir pressure drops below the AOP, asphaltene molecules start to aggregate. Because the polarity of asphaltene molecules is high, water films start to destabilize and eventually rupture, allowing the crude oil to contact the rock surface. The polar ends of the asphaltene molecules adsorb onto the rock, exposing the hydrocarbon end and making the surface more oil-wet (Anderson, 1986).

Table 2—ANALYSIS OF PRODUCED WATER

Cation	mg/litre	Anion	mg/litre
Na^+	1,613	Cl^-	1,978
K^+	66	Br^-	12
Ca^{2+}	35	HCO_3^-	914
Mg^{2+}	1	OH^-	0
NH^{4+}	15	CO_3^{2-}	6
Total Fe	0	SO_4^{2-}	72
		$KMnO_4$	789
		HBO_3^{2-}	235
		Total Dissolved Solids:	5,737 ppm
		Density:	1.001g/cc

We have seen that Well B's asphaltene precipitation tendency is severe and that the asphaltene molecules are polarized, while the original wettability of the clay-rich sandstone reservoir is inferred to be water-wet. Both fluid and rock properties facilitate a favorable environment for the wettability to change when the reservoir pressure drops below the AOP. For this reason, we hypothesized that the cause of the rapid water cut increase was caused by an increase in the water relative permeability as a result of the wettability alteration by asphaltene deposition. We built a dynamic simulation model that includes the effect of asphaltene and compared the calculated result with the field data to test this hypothesis.

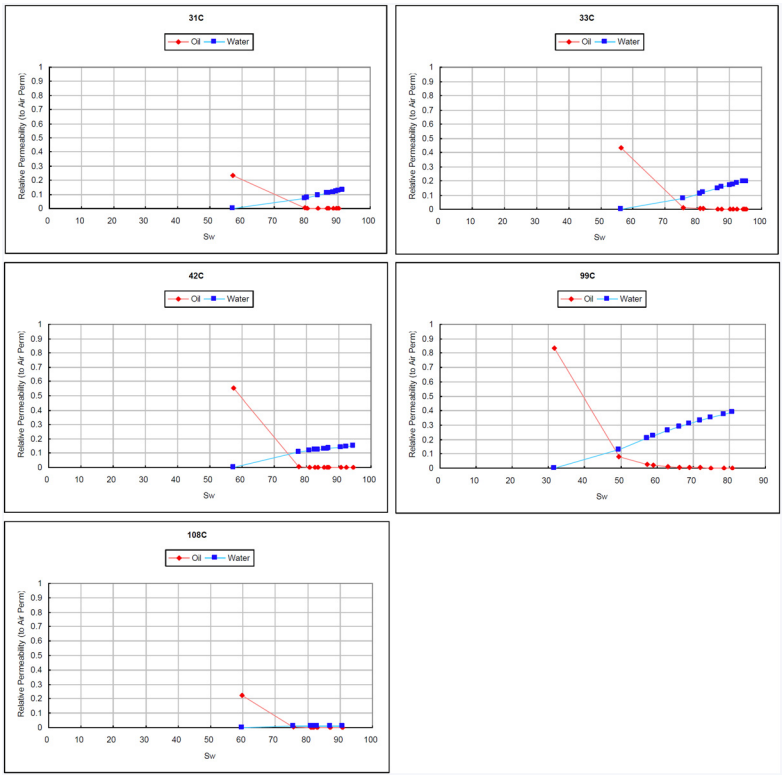

Figure 14—Water-displacing-oil relative permeability curves from five restored-state core samples. Original wettability of the reservoir rock was inferred to be water-wet based on the shape of these curves.

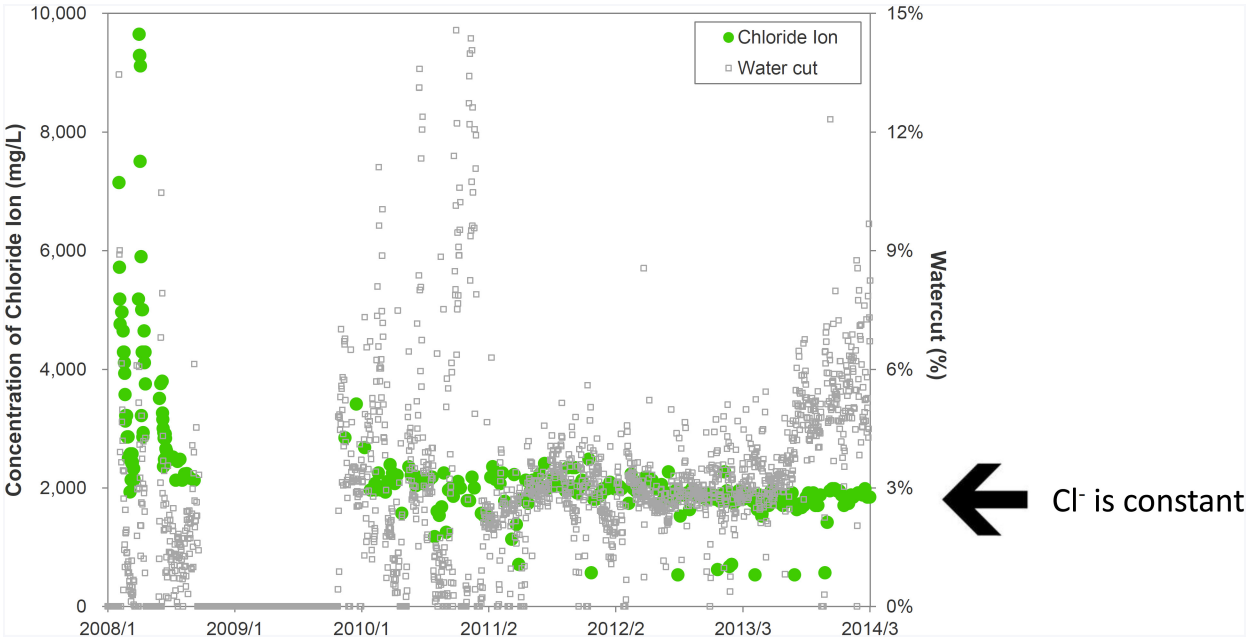

Figure 15—Concentration of chloride ions in the produced water since the production startup in 2008. The constant concentration indicated that the ingress of water from behind the casing is unlikely. High salinity in early 2008 is due to cleanup of the KCl brine.

Numerical Investigation

Base Model

We built a 20x1x7 single well radial dynamic flow simulation model for this study (**Fig. 17**). The model can match the history (both pressure and water cut) from 2011 to 2012 when the reservoir demonstrated

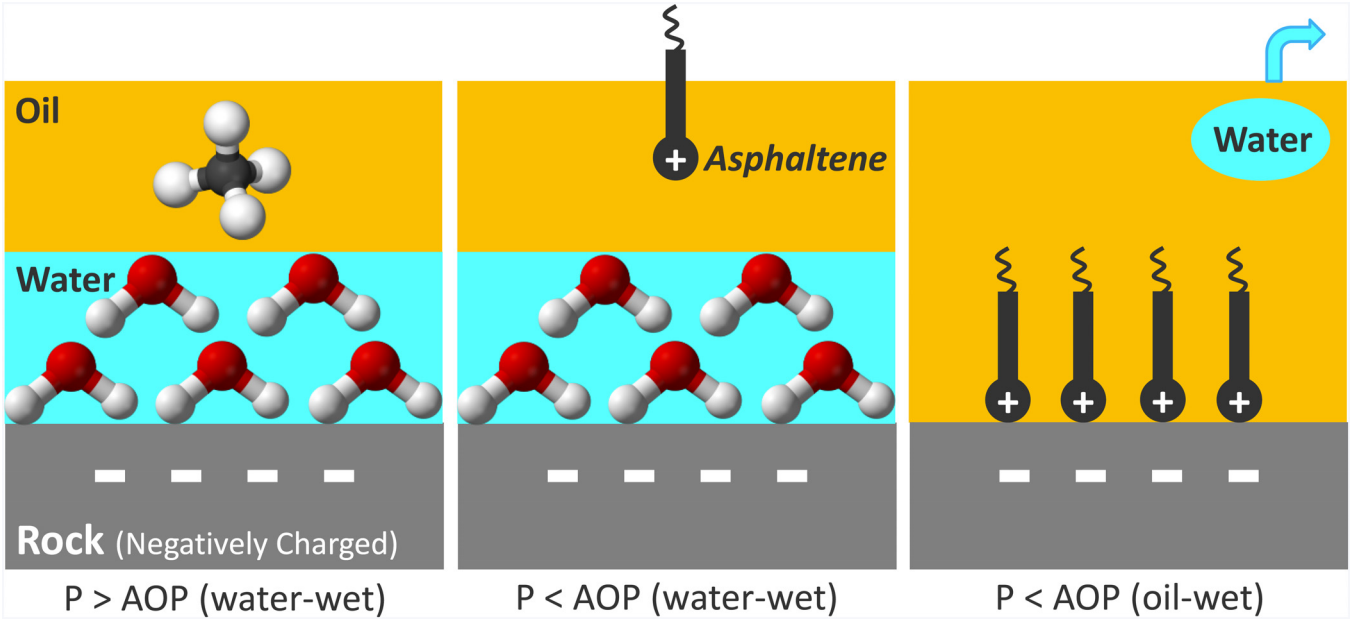

Figure 16—Mechanism of wettability alteration by asphaltene deposition. The negatively charged rock surface is initially covered by a water film (left). While pressure is greater than the AOP, asphaltene is not precipitated and the oil polarity is low. When pressure is less than the AOP, asphaltene starts to precipitate. Asphaltene has both polar and hydrocarbon ends, and water films start to become unstable (middle). At some point, the water films rupture and asphaltene adsorbs onto the rock surface, reducing the irreducible water saturation. The surface becomes more oil-wet because the hydrocarbon ends of the asphaltene molecules are exposed (right).

Table 3—FLUID COMPOSITION

Component	Mol%	Molecular Weight (gm/gmol)	Critical Pressure (kg/cm^2)	Critical Temperature (K)	Acentric Factor
CO2	0.27	44.0	72.8	304.2	0.225
N2-C1	26.93	16.1	45.3	190.2	0.0082
C2	6.80	30.1	48.2	305.4	0.098
C3	8.37	44.1	41.9	369.8	0.152
C4	5.97	58.1	37.1	421.0	0.189
C5	3.95	72.2	33.3	465.4	0.240
C6	5.47	84.9	31.3	515.5	0.280
C7-C8	11.22	105.5	30.1	556.7	0.329
C9-C11	9.87	138.1	25.1	620.2	0.434
C12-C15	8.96	180.4	20.1	688.9	0.577
C16-C20	5.66	246.9	15.8	757.7	0.749
C21-C30	4.72	340.6	12.1	828.3	0.953
C31+	1.83	530.3	8.44	936.9	1.204

Table 4—PROPERTIES OF FORMATION WATER AND ROCK

Reference Pressure	5,000 (psia)
Formation Volume Factor	1.03 (RB/STB)
Water Compressibility	3.6E-06 (1/psi)
Water Viscosity	0.23 (cP)
Rock Compressibility	4.28E-06 (1/psi)

a pseudo-steady state and most of the well shut-in pressures from 2008 to 2014, indicating that the reservoir size has been modeled correctly. However, the match with the history since early 2013 is unsatisfactory. We identified a clear discrepancy between the measured data and the simulation result in both pressure and water cut. Composition of the hydrocarbon fluid, properties of formation water and rock, and properties of simulation grids are summarized in **Tables 3** to **5**. The free water level (FWL) lies 50 meters below the deepest production interval. This bottom cell is in the oil-water transition zone,

Table 5—PROPERTIES OF THE SIMULATION GRIDS

Layer	Porositys (fraction)	Absolute Permeabilitys(mD)	Thicknesss(m)	Irreducible Water Saturation (Critical Water Saturation)	Residual Oil Saturaiton
Layer 1	0.149	2.4	12	0.5253	0.1506
Layer 2	0	0	3	No value	No value
Layer 3	0.143	2.3	13	0.5296	0.1767
Layer 4	0	0	5	No value	No value
Layer 5	0.133	1.8	12	0.5453	0.2202
Layer 6	0	0	43	No value	No value
Layer 7	0.137	3.3	9	0.5034	0.2028

while the upper three layers are in the oil pay zone. The model does not have an aquifer. The history-matched model suggests that the majority of the water production comes from the transition zone, and that the gradual increase in water cut is mainly due to expansion of the water. The next modeling challenge was to obtain a history match from early 2013 onward, in which productivity dropped and water cut increased. No effort was made to match the period between 2008 and 2010 because the low productivity was caused by the well stimulation failure, which was not a natural phenomenon.

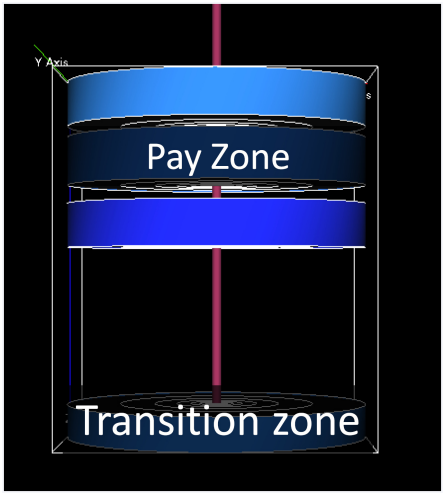

Figure 17—View of a single well radial reservoir simulation model (20x1x7). The bottom layer is in the oil-water transition zone, while the upper three layers are in the oil pay zone (water saturation is equal to the critical water saturation and the irreducible water saturation). The model does not have an aquifer.

Possible Suspects Other than Asphaltene

Before introducing the effect of asphaltene into the simulator, we examined the following three non-asphaltene related parameters: (i) attachment of a weak aquifer, (ii) changing the shape of the water relative permeability curves, and (iii) changing the value of the water compressibility. However, no satisfactory match was obtained. In particular, it proved difficult to match the rapid water cut increase seen since early 2013. Hence, these parameters were excluded from the investigation. In the next step, we included the effect of asphaltene into the model.

Modeling Asphaltene Damage

This section describes the modeling of formation damage (reduction in porosity and permeability) caused by asphaltene precipitation. Asphaltene is characterized by three additional components in the simulator: precipitation, flocculation and deposition (Schlumberger 2012; Fadili et al. 2009; Boek et al. 2011).

Precipitation Asphaltene remains dissolved in the oil phase when pressure is above the AOP. However, once the reservoir pressure drops below the AOP, asphaltene particles begin to precipitate. Solubility is modeled as a function of pressure in the simulator, which was based on the experimental data from the filtration test. The AOP was initially set to 3,410 psia, but it was later adjusted to 3,900 psia to better match the history and to account for the pressure difference between the well pressure and the block pressure in the simulation model.

Flocculation Once precipitation occurs, the fine particles of asphaltene aggregate to form larger particles called “flocs”. The flocculation reaction rate is given by:

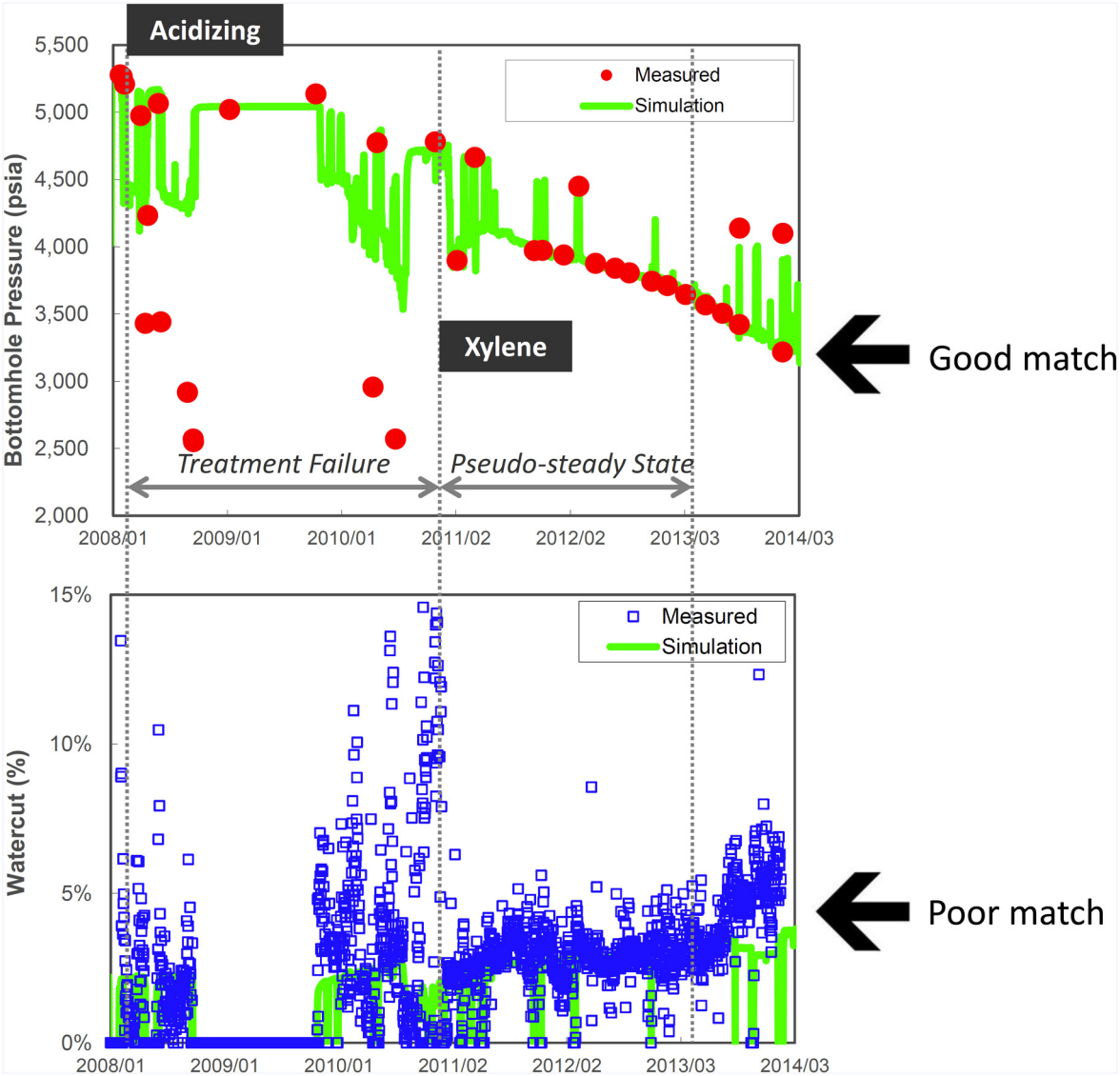

Figure 18—Simulation results from a model that includes the effect of reduction in porosity and permeability. The match with the pressure decline from early 2013 is improved but the match with the water cut is still unsatisfactory. Red dots represent measured pressure. Blue dots represent daily measured water cut. Green lines represent simulation results.

$$R_f = V_f r_f \frac{m_{wp}}{m_{woil}} C_{pf} \tag{2}$$

where R_f is the flocculation rate, V_f is the fluid volume, r_f is the kinetic reaction rates for the flocculation of fines into "flocs", m_{wp} is the molecular weight of the precipitation component, m_{woil} is the molecular weight of the oil, and C_{pf} is the concentration of the fines in the oil phase. We treated r_f as a matching parameter and a value of 10 (1/day) was used.

Deposition After the asphaltene components coalesce to form flocs, they can be adsorbed onto the rock surface (adsorption), block the pore throats (plugging), or be flushed away by oil flow (entrainment). These mechanisms are described using the following deep bed filtration model (Wang and Civian 2001):

$$\frac{\partial E_A}{\partial t} = \alpha V_f C_f - \beta V_f (U_o - U_{cr}) S_o S_s + \gamma F_o L (C_f - C_{fcr}) \tag{3}$$

where E_A is the fractional volume occupied by the asphaltene deposits, α is the adsorption coefficient, C_f is the concentration of the flocs in the oil phase (flowing flocs), β is the entrainment coefficient, U_o

is the average oil velocity, U_{cr} is the critical velocity for entrainment, S_o is the oil saturation, S_s is the solid (asphaltene) saturation, γ is the plugging coefficient, F_o is the average oil flow rate, L is the length of the flow path, and C_{fcr} is the critical concentration of flocs for plugging to occur. We used $\alpha=0$, $\beta=0$, $\gamma=1$ (1/ft) and $C_{fcr}=0$.

Porosity Reduction Asphaltene deposition reduces the porosity. The reduced porosity is equal to the difference between initial porosity and the fractional pore volume occupied by the asphaltene deposits:

$$\emptyset = \emptyset_0 - E_A \tag{4}$$

where φ is the instantaneous porosity, and φ_0 is the initial porosity.

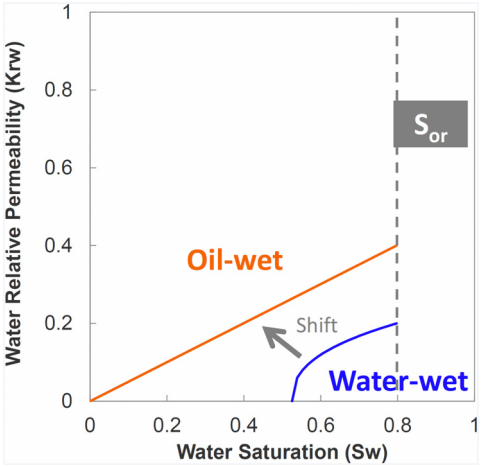

Figure 19—Effect of wettability alteration on water relative permeability curve. Both critical water saturation and maximum water saturation are shifted. The blue curve represents the water relative permeability under water-wet (initial state). The orange line represents the water relative permeability after alteration to oil-wet (final state).

Permeability Reduction Asphaltene deposition also reduces the permeability. Reduced permeability is correlated to the porosity using a power law:

$$\mathrm{k} = k_0 \left(\frac{\emptyset}{\emptyset_0}\right)^m \tag{5}$$

where k is the instantaneous permeability, k_0 is the initial permeability, and m is the power law exponent. Due to the absence of asphaltene core flood deposition experiments, we used $m=5$ as a matching parameter.

A reasonable match was obtained after including the effect of asphaltene to reduce porosity and permeability, as shown in **Fig. 18**. The pressure match since early 2013 has improved, however, the water cut match is still unsatisfactory. Some modifications to the water relative permeability are required to match the water cut.

Modeling Wettability Change

Wettability change was captured by a shift in the water relative permeability curve, as illustrated in **Fig. 19**. First, the critical water saturation was scaled:

$$S_{wcr} = FS_{wcra} + (1-F)S_{wcri} \tag{6}$$

where S_{wcr} is the instantaneous critical water saturation, F is the weighting factor determined as a function of the solid (asphaltene) saturation, S_{wcra} is the critical water saturation when oil-wet (final state), and S_{wcri} is the critical water saturation when water-wet (initial state).

And second, the maximum water relative permeability was scaled:

$$k_{rw} = Fk_{rwa} + (1-F)k_{rwi} \tag{7}$$

where k_{rw} is the instantaneous water relative permeability, k_{rwa} is the water relative permeability when oil-wet (final state), and k_{rwi} is the water relative permeability when water-wet (initial state). The critical water saturation and the irreducible water saturation in the final state water relative permeability table were set to zero, while the maximum water relative permeability at the residual oil saturation was set to 0.4. The two end points were connected by a straight line due to lack of water relative permeability experiment at the oil-wet state. The weighting factor was set to $F=0$ when the solid saturation is zero, and $F=1$ when the solid saturation is 0.3.

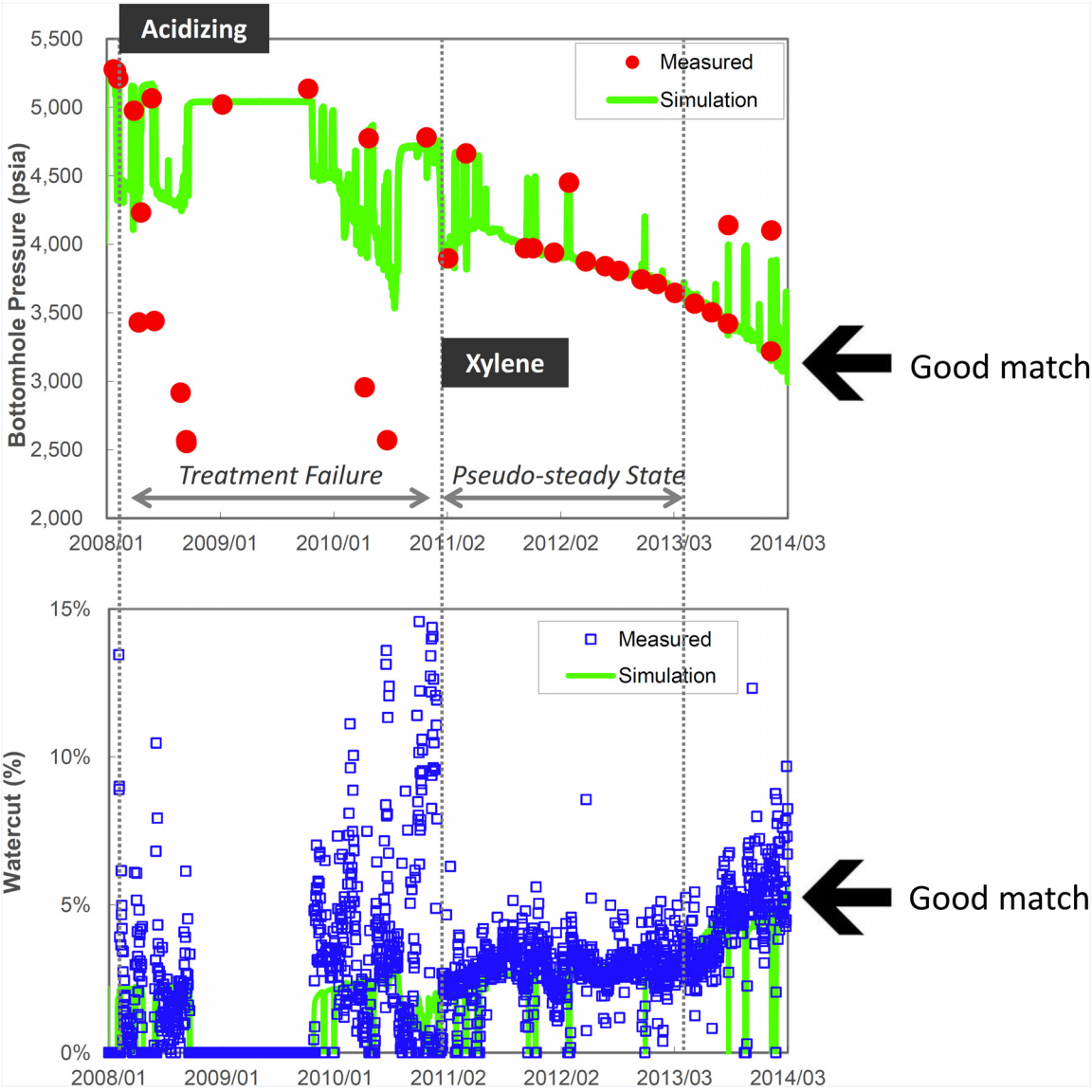

Figure 20—History-match obtained after including the effect of asphaltene damage and the wettability alteration. Both pressure decline and water cut increase were well matched. Red dots represent measured pressure. Blue dots represent daily measured water cut. Green lines represent simulation results.

The simulation result including the effect of asphaltene damage and wettability alteration demonstrated an excellent match in both pressure and water cut (**Fig. 20**), which numerically validated our hypothesis.

Conclusions

The main conclusions of this study are:

- The decline in productivity from 2008 to 2010 was mostly linked to the acid stimulation failure. The well productivity recovered because the asphaltene sludges were removed by xylene in January 2011.
- The decline in productivity since early 2013 can be explained by formation damage caused by asphaltene precipitation associated with a decline in reservoir pressure below the AOP.
- The rapid increase in water cut can be explained by the increase in water relative permeability as a result of wettability alteration by asphaltene deposition.

Acknowledgments

The author thanks INPEX Corporation for granting the permission to publish this work. Professor Toshifumi Matsuoka and Assistant Professor Yunfeng Liang from Kyoto University are appreciated for kindly providing with Fig. 12.

References

Akbarzadeh, K., Hammami, A., et alet al. 2007. Asphaltenes – Problematic but Rich in Potential. *Oilfield Review* September 2007: 22–43.

Anderson, W. 1986. Wettability Literature Survey - Part 1: Rock/Oil/Brine Interactions and the Effects of Core Handling on Wettability. *Journal of Petroleum Technology* **38**(10): 1125–1144. SPE-13932-PA. http://dx.doi.org/10.2118/13932-PA.

Anderson, W. 1987. Wettability Literature Survey - Part 5: The Effects of Wettability on Relative Permeability. *Journal of Petroleum Technology* **39**(11): 1453–1468. SPE-16323-PA. http://dx.doi.org/10.2118/16323-PA.

Brown, J. K.; Ladner, W. R. Hydrogen distribution in coal-like material by high resolution NMR Spectroscopy, II. A comparison with infrared measurement and the conversion to carbon structure. *Fuel* 1960, **39,** 87–96.

Craig, F. 1993. *The Reservoir Engineering Aspects of Waterflooding,* Vol. **3,** 19–21. Monograph Series, SPE.

Boek, E., Fadili, A., Williams, M., and Padding, J. 2011. Prediction of Asphaltene Deposition in Porous Media by Systematic Upscaling from a Colloidal Pore Scale Model to a Deep Bed Filtration Model. Paper SPE 147539 presented at the SPE Annual Technical Conference and Exhibition, Denver, Colorado, USA, 30 October-2 November. http://dx.doi.org/10.2118/147539-MS.

Fadili, T., Ibrahim, M., and Al-Matar, B. 2009. Modeling The Effect Of Asphaltene on the Development of the Marrat Field. Paper SPE 120988 presented at the 8th European Formation Damage Conference, Scheveningen, The Netherlands, 27-29 May. http://dx.doi.org/10.2118/120988-MS.

Hammami, A. and Ratulowski, J. 2007. Precipitation and Deposition of Asphaltenes in Production Systems: A Flow Assurance Overview. In *Asphaltenes, Heavy Oils, and Petroleomics,* ed. O. Mullins, E. Sheu, A. Hammami and A. Marshall, Chap. 23, 617–660. New York City: Springer.

Hibi, R., Tagami, L., Kobayashi, K., Liang, Y., Honda, H., Murata, S., Matsuoka, T., Morimoto, M., Uetani, T., and Boek, E. 2014. Investigation of asphaltene-asphaltene association and aggregation for compositional reservoir simulators by quantitative molecular representations. Paper IPTC 18097 presented at the International Petroleum Technology Conference, Kuala Lumpur, Malaysia, 10-12 December.

Jamaluddin, A., Creek, J., Kabir, C., McFadden, J., D'Cruz, D., Manakalathil, J., Joshi, N., and Ross, B. Laboratory Techniques to Measure Thermodynamic Asphaltene Instability. *Journal of Canadian Petroleum Technology* **41**(07): 44–52. PETSOC 02-07-04. http://dx.doi.org/10.2118/02-07-04.

Kaminsky, R. and Radke, C. 1997. Asphaltenes, Water Films, and Wettability Reversal. *SPE Journal* **2**(04): 485–493. SPE-39087-PA. http://dx.doi.org/10.2118/39087-PA.

Kokal, S., Al-Dawood, N., Fontanilla, J., Al-Ghamdi, A., Nasr-El-Din, H., and Al-Rufaie, Y. 2003. Productivity Decline in Oil Wells Related to Asphaltene Precipitation and Emulsion Blocks. *SPE Production & Facilities* **18**(4): 247–256. SPE-87088-PA. http://dx.doi.org/10.2118/87088-PA.

Kokal, S., Sayegh, S. 1995. Asphaltenes: The Cholesterol of Petroleum. Paper SPE 29787 presented at the Middle East Oil Show, Bahrain, 11-14 March. http://dx.doi.org/10.2118/29787-MS.

Leontartis, K. and Mansoori, A. 1987. Asphaltene Deposition: A Survey of Field Experiences and Research Approaches. *Journal of Petroleum Science and Engineering* **1**(1988): 229–239.

Mansoori, G. Asphaltene deposition: an economic challenge in heavy petroleum crude utilization and processing. 1988. *OPEC Review* **12**(1): 103–113.

Morgan, J. and Gordon, D. 1970. Influence of Pore Geometry on Water-Oil Relative Permeability. *Journal of Petroleum Technology,* Vol. **22**(10), 1199–1208. Richardson, Texas: Society of Petroleum Engineers. http://dx.doi.org/10.2118/2588-PA.

Nghiem, L. and Kohse, B. 2006. *Asphaltenes and Waxes,* Volume **1,** 427–429. Richardson, Texas: Petroleum Engineering Handbook, SPE.

Pallatt, N., and Thornley, D. 1990. The Role of Bound Water and Capillary Water in the Evaluation of Porosity in Reservoir Rocks. In *Advances in Core Evaluation,* ed. P. Worthington, 223–237. Amsterdam: Reviewed proceedings of the First Society of Core Analysis, European Core Analysis Symposium.

Pedroza, T., Calderon, G., and Rico, A. 1996. Impact of Asphaltene Presence in Some Rock Properties. *SPE Advanced Technology Series* **4**(01): 185–191. SPE-27069-PA. http://dx.doi.org/10.2118/27069-PA.

Schlumberger. *Eclipse Reservoir Engineering Software*. 2012. http://www.software.slb.com/products/foundation/pages/eclipse.aspx/ (accessed 01 August 2014).

Tagami, K., Hibi, R., Liang, Y., Honda, H., Matsuoka, T., Morimoto, M., Uetani, T., and Boek, E. 2014. Quantitative molecular representation of asphaltenes and heavy fractions for digital oil. 2014. Poster presentation given at the 15th International Conference on Petroleum Phase Behavior and Fouling, Galveston, Texas, USA, 8-12 June.

Tongchun, Y., Fadili, A., Muhammad, I., Ibrahim, N., and Al-Matar, B. 2009. Modeling The Effect Of Asphaltene on the Development of the Marrat Field. SPE 120988 presented at 8th European Formation Damage Conference, Scheveningen, The Netherlands, 27-29 May. http://dx.doi.org/10.2118/120988-MS.

Uetani, T. Matsuoka, T. and Honda, H. 2014. Removal of Plugged Asphaltene in a Reservoir by Earthquakes. Paper SPE 168137 presented at the SPE International Symposium and Exhibition on Formation Damage Control, Lafayette, Louisiana, USA, 26-28 February. http://dx.doi.org/10.2118/168137-MS.

Wang, S. and Civian, F. 2001. Productivity Decline of Vertical and Horizontal Wells by Asphaltene Deposition in Petroleum Reservoirs. Paper SPE 64991 presented at the SPE International Symposium on Oilfield Chemistry, Houston, Texas, 13-16 February. http://dx.doi.org/10.2118/64991-MS.

Yen, A., Ralph Yin, Y., and Asomaning, S. 2001. Evaluating Asphaltene Inhibitors: Laboratory Tests and Field Studies. Paper SPE 65376 presented at the SPE International Symposium on Oilfield Chemistry, Houston, Texas, 13-16 February.